Reynolds and Mach number effects in compressible **turbulent** channel flow

Davide Modesti and Sergio Pirozzoli

Dipartimento di Ingegneria Meccanica e Aerospaziale, Università di Roma 'La Sapienza', via Eudossiana 18, 00184 Roma, Italia

Abstract

The effect of Reynolds and Mach number variation in compressible isothermal channel flow is investigated through a series of direct numerical simulations (DNS), at bulk Mach number $M_b = 1.5, 3$ and bulk Reynolds number up to $Re_b = 34000$, which is sufficient to sense sizeable high-Reynolds-number effects not reached before in this type of flow. Dedicated incompressible DNS are also performed at precisely matching Reynolds number, to directly gauge the performance of compressibility transformations for the mean velocity profiles and Reynolds stresses. As in previous studies, we find inaccuracy of the classical van Driest transformation to remove effects of variable density and viscosity, especially at low Reynolds number. On the other hand, almost perfect matching of incompressible mean velocity and Reynolds stress distributions is recovered throughout the wall layer by using a recently introduced transformation [1, 2], the only remaining effect of compressibility being the increase of the streamwise turbulence intensity peak with the Mach number. Temperature/velocity relations are scrutinized, with the main finding that a recent relation by Zhang et al. [3], which explicitly accounts for finite wall heat flux, is more accurate than the classical Walz relation. The size of the typical turbulent eddies is studied through spanwise spectral densities of the velocity field, which support validity of a scaling based on the local mean shear and the local friction velocity, with the main conclusion that the actual size of the eddies does not vary with the Mach number, at a fixed outer wall distance.

Keywords: Compressible flow, Wall turbulence, Direct Numerical Simulation

1. Introduction

Compressible wall-bounded turbulent flows are of obvious importance in aerospace applications and have been extensively studied in the past, although some basic issues as Mach and Reynolds number effects on the mean velocity profile and on the Reynolds stresses distribution are not yet fully settled. Most early studies were based on experimental approaches, as thoroughly reviewed by Bradshaw [4], Smits and Dussauge [5], Gatski and Bonnet [6]. However, growth of available computational power has recently made the numerical solution of the full compressible Navier-Stokes equation feasible, and direct numerical simulation (DNS) has become an important tool in turbulence research. The effects of finite flow compressibility on turbulence have been traditionally divided into indirect effects due to mean density and temperature variations, and genuine effects caused by dilatational velocity fluctuations and thermodynamic fluctuations. Morkovin [7] postulated that for non-hypersonic boundary layers (say, $M < 5$), genuine effects of compressibility are negligible, hence the mean flow profiles are expected to collapse to the corresponding incompressible distributions, provided mean density and viscosity variations are suitably taken into account. Morkovin's hypothesis also subtends earlier theoretical findings, as the celebrated van Driest transformation for the mean velocity profile [8], and led to relations between temperature and velocity fluctuations for adiabatic boundary layers, collectively known as strong Reynolds analogies (SRA) [7, 9, 10]. Many studies of compressible boundary layers support the validity of Morkovin's hypothesis, at least for adiabatic walls, whereas the original SRA relationships turned out not be very robust [11, 12, 3].

Planar channel is the simplest prototype of wall-bounded internal flows. Since the pioneering work of Kim et al. [13], many DNS studies of incompressible channel flows have appeared, and Reynolds numbers have been reached at which a sizeable layer with near-logarithmic variation of the mean velocity emerges [14, 15, 16]. Pioneering studies of turbulent channel flow at supersonic conditions ($M_b = 1.5$, $Re_b = 3000$ being the bulk Mach ad Reynolds number, respectively) were carried out by Coleman et al. [17], Huang et al. [10]. Those authors studied compressible channel flows between isothermal walls, in which the wall is necessarily cooler than the bulk fluid, and found that the van Driest-transformed velocity follows only approximately the incompressible law-of-the-wall, with differences attributed to low-Reynolds-number effects. Those authors also showed that density

and temperature fluctuations are indeed small as compared to their mean values, thus substantiating Morkovin's hypothesis. The turbulent stresses were found to collapse fairly well on incompressible data when scaled with the mean density ratio, but better agreement was observed when 'semi-local' units are used, based on a local friction velocity and viscous length scale. Lechner et al. [18] reproduced the flow case considered by Coleman et al. [17] using a pressure-velocity-entropy formulation with governing equations cast in characteristic form, and discretized with fifth-order compact upwind formulas. Good agreement was observed with the results of Coleman et al. [17], and higher values of the density-scaled normal Reynolds stresses were observed as compared to the incompressible case, whereas the transformed turbulent shear stress was found to be lower. Morinishi et al. [19], Tamano and Morinishi [20] carried out DNS of compressible channel flow between both isothermal and adiabatic walls using a Fourier/Galerkin B-spline discretization [21], confirming the validity of Huang's semi-local scaling for the turbulent stresses. Foysi et al. [22] performed DNS spanning bulk Mach numbers in the range between 0.3 and 3.5. Consistent with previous works, they found that the density-scaled turbulent stresses collapse on the incompressible distributions sufficiently far from the wall when reported in outer scaling, whereas Huang's semi-local scaling yields better accuracy than van Driest in inner scaling. Brun et al. [23] developed an extensive large-eddy simulation database of compressible channel flows, and noticed that as the Mach number is increased for given bulk Reynolds number the flow tends to relaminarize, although the friction Reynolds number increases, thus raising the important question of which is the relevant Reynolds number for comparing flow cases across the Mach number range. Brun et al. [23] also proposed a modified form of mean velocity scaling which explicitly takes into account mean viscosity variations, and which was found to yield better collapse on incompressible data than semi-local scaling. Wei and Pollard [24, 25] used a discontinuous Galerkin solver to develop a DNS dataset of compressible channel flows spanning the bulk Mach number range between 0.2-1.5. As in previous studies, they found that as the bulk Mach number increases the transformed turbulent stresses do not follow the incompressible profiles when reported in wall units. In a recent work, Trettel and Larsson [1, 2] further investigated failure of the van Driest transformation in the case of cold walls. They showed that the semi-local scaling of Huang et al. [10] is actually rooted in arguments of mean momentum balance, and they derived a novel velocity transformation which by construction satisfies universality of the turbulent

stresses. The novel transformation was shown to yield satisfactory agreement of the mean velocity profiles with incompressible distributions in a reasonably wide range of Reynolds and Mach numbers. One of the uses of 'compressibility transformations' consists in the derivation of predictive relations for the friction coefficient, such as the popular van Driest II transformation [26]. In order to derive such friction relations a temperature-velocity relation is also needed. For that purpose, one popular choice is Walz relation [27], which has been found to work well for adiabatic boundary layers [28, 29]. An empirical correction to Walz formula was proposed by Duan and Martin [30], and generalized by Zhang et al. [3], to explicitly account for finite wall heat flux.

A frequently debated issue in the compressible flow community is the effect of flow compressibility on the typical length scales in wall turbulence [31, 5]. Although there is a general consensus that the integral scales of fluid motion sufficiently away from the wall do not vary substantially with the Reynolds number, the dependence on the Mach number is still largely unclear. Furthermore, most available experimental data only refer to the streamwise length scales, which can be easily estimated from one-point measurements, upon use of Taylor's hypothesis. In this respect, Demetriades and Martindale [32] found that the streamwise integral length scales in a Mach 3 boundary layer are about half as in incompressible boundary layers. Smits et al. [33] also observed that the streamwise length scales sensibly decrease with the Mach number, whereas the spanwise length scales are almost unchanged. On the other hand, Spina et al. [31] claimed that the integral length scales increase with the Mach number both in inner and outer units, being weakly affected by the Reynolds number. Recent measurements by Ganapathisubramani et al. [34] at M = 2 seem to suggest substantial increase of the eddy size in both the streamwise and in the spanwise direction with the Mach number, whereas recent DNS [12] at M = 2 support insensitivity on the Mach number, at least for adiabatic boundary layers.

To shed some light on the open issues outlined above, we have developed a novel database of compressible channel flow in the range of bulk Mach numbers from $M_b = 1.5$ to 3, and bulk Reynolds numbers up to $Re_b \approx 34000$, which significantly extends the range of previous DNS. In order to precisely gauge the importance of compressibility effects and directly assess the validity of the compressibility transformations, a series of companion incompressible DNS have been performed so as to exactly match the relevant Reynolds number (see the later discussion), thus avoiding ambiguities/uncertainties of

previous studies.

2. DNS setup

We solve the Navier-Stokes equations for a perfect heat-conducting gas

$$\frac{\partial \rho}{\partial t} + \frac{\partial \rho u_i}{\partial x_i} = 0, \tag{1a}$$

$$\frac{\partial \rho u_i}{\partial t} + \frac{\partial \rho u_i u_j}{\partial x_j} = -\frac{\partial p}{\partial x_i} + \frac{\partial \sigma_{ij}}{\partial x_j} + f\delta_{i1}, \tag{1b}$$

$$\frac{\partial \rho E}{\partial t} + \frac{\partial \rho u_j H}{\partial x_j} = -\frac{\partial q_j}{\partial x_j} + \frac{\partial \sigma_{ij} u_i}{\partial x_j} + f u_1, \tag{1c}$$

where u_i, $i = 1, 2, 3$, is the velocity component in the i-th direction, ρ the density, p the pressure, $E = c_v T + u_i u_i/2$ the total energy per unit mass, and $H = E + p/\rho$ is the total enthalpy. $\gamma = c_p/c_v = 1.4$ is the specific heat ratio. q_j and σ_{ij} are the components of the heat flux vector and the viscous stress tensor respectively,

$$\sigma_{ij} = \mu \left(\frac{\partial u_i}{\partial x_j} + \frac{\partial u_j}{\partial x_i} - \frac{2}{3} \frac{\partial u_k}{\partial x_k} \delta_{ij} \right), \tag{2}$$

$$q_j = -k \frac{\partial T}{\partial x_j}, \tag{3}$$

where the dependence of the viscosity coefficient on temperature is accounted for through Sutherland's law and $k = c_p \mu / Pr$ is the thermal conductivity, with $Pr = 0.72$. The forcing term f in equation (1b) is evaluated at each time step in order to discretely enforce constant mass-flow-rate in time, and the corresponding power spent is added to the right-hand-side of the total energy equation. The nonlinear terms in the Navier-Stokes equations are discretized using central sixth-order locally conservative, energy-consistent formulas which guarantee that the total kinetic energy is discretely conserved in the limit case of inviscid incompressible flow [35]. This approach avoids the introduction of any artificial viscosity for numerical stabilization, as done in most existing compressible flow solvers. The viscous terms are expanded to Laplacian form and also approximated with sixth-order formulas, to avoid odd-even decoupling phenomena. Time advancement is carried out by means of an explicit third-order low-storage Runge-Kutta algorithm.

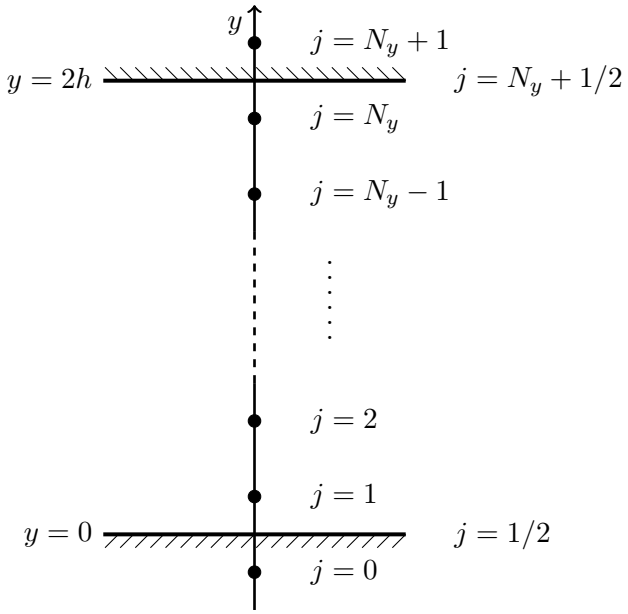

Figure 1: Distribution of collocation points in wall-normal direction. Walls are made to coincide with the intermediate nodes $j = 1/2$, $j = N_y + 1/2$, where the numerical convective fluxes are set to zero.

The DNS are carried out in a rectangular box whose size in the x, y, z coordinate directions is $6\pi h \times 2h \times 2\pi h$, where h is the channel half-height. This relatively large size as compared to previous studies is dictated by the need to accommodate the large eddies which become energetically relevant at sufficiently high Reynolds number [14, 15]. The mesh spacing is constant in the wall-parallel directions, and an error-function mapping is used to cluster mesh points towards the walls. As for the boundary conditions, periodicity is enforced in the homogeneous wall-parallel directions, and no-slip isothermal conditions are imposed at the channel walls. In this respect, we note that the presence of the walls in y direction may lead to failure in the conservation of mass in co-located flow solvers [17, 19, 17], which is typically fixed by adding a source term to the continuity equations at the wall nodes in such a way that the integrated density remains discretely constant in time. In this work we prefer to stagger the first node off the wall in such a way that the latter coincides with an intermediate node (see figure 1), where the convective fluxes are identically zero. Hence, correct telescoping of the numerical fluxes is guaranteed, and no net mass variation can occur. A further benefit of this approach is that, for given distance of the first grid point from the wall, the maximum allowable time step associated with the vertical mesh spacing is doubled. In order to maximize the spectral resolution in the streamwise direction, all simulations are performed in a convective frame of reference [36], in which the bulk velocity is zero. All computations are initiated with a parabolic velocity profile with superposed random perturbations, and with uniform values of density and temperature.

Both Reynolds ($\phi = \overline{\phi} + \phi'$) and Favre ($\phi = \widetilde{\phi} + \phi''$, $\widetilde{\phi} = \overline{\rho\phi}/\overline{\rho}$) decompositions will be used in the following, where the overline symbol denotes averaging in the homogeneous space directions and in time. Bulk Reynolds and Mach number are defined as $Re_b = 2\rho_b u_b h/\mu_w$, $M_b = u_b/c_w$, where $\rho_b = 1/V \int_V \rho \mathrm{d}V$ is the bulk density, and $u_b = 1/(\rho_b V) \int_V \rho u \mathrm{d}V$ is the bulk velocity in the channel (both exactly constant in time), and μ_w and c_w are the dynamic viscosity coefficient and the speed of sound at the wall temperature, respectively. For notational clarity, components of the Reynolds stress tensor are denoted as $\tau_{ij} = \widetilde{u_i'' u_j''}$, and quantities made nondimensional with respect to the wall friction velocity ($u_\tau = \sqrt{\tau_w/\rho_w}$) and the viscous length scale ($\delta_v = \nu_w/u_\tau$, where $\nu = \mu/\rho$ is the kinematic viscosity), are denoted with the '+' superscript. The friction Reynolds number is defined as the ratio of outer to viscous length scales, hence $Re_\tau = h/\delta_v$. Details on the

Case	Re_b	M_b	Re_τ	$Re_{\tau H}$	$Re_{\tau B}$	N_x	N_y	N_z	Δx^+	Δz^+	M_τ	$-B_q$
CH01	5790	0.1	180	180	180	384	128	192	8.8	5.9	0.0063	9.7e-6
CH15A	6000	1.5	215	141	169	512	128	256	8.0	5.2	0.079	0.048
CH15B	15334	1.5	500	333	395	1024	256	512	9.2	6.1	0.072	0.042
CH15C	34000	1.5	1015	677	802	2048	512	1024	9.3	6.2	0.065	0.038
CH3	9760	3.	448	142	233	1024	256	512	8.2	5.5	0.11	0.14
CH15M	6000	1.5	218	141	169	120	180	120	23	7.6	0.079	0.048
CH15MF	6000	1.5	215	141	169	256	128	128	10	7.0	0.079	0.048

Table 1: Setup of compressible channel DNS. The computational box size is $6\pi h \times 2h \times 2\pi h$ for all flow cases, except case CH15M, which reproduces the DNS of Morinishi et al. [19], and CH15MF with improved spatial resolution, in which the box size is $4\pi h \times 2h \times 4/3\pi h$. N_i and Δx_i^+ are the number of points and the mesh spacing in the i-th coordinate direction, respectively. $M_\tau = u_\tau/c_w$ is the friction Mach number, and $B_q = q_w/(\rho_w C_p u_\tau T_w)$ is the heat flux coefficient. $Re_{\tau I}$ is the equivalent friction Reynolds number for Huangs' transformation (H), and Brun's transformation (B), as defined in equation (15).

Case	Re_b	Re_τ	N_x	N_y	N_z	Δx^+	Δz^+
INC1	4272	140	384	128	192	6.9	4.6
INC2	5248	169	384	128	192	8.3	5.5
INC3	5790	180	384	128	192	8.8	5.9
INC4	7082	222	384	128	192	11	7.3
INC5	10074	299	768	192	384	7.3	4.9
INC6	13774	393	1024	256	512	7.2	4.8
INC7	20062	550	1024	256	512	10	6.7
INC8	25534	673	2048	512	1024	6.2	4.1
INC9	30800	796	2048	512	1024	7.3	4.9
INC10	39600	999	2048	384	1024	9.2	6.1

Table 2: Setup of incompressible channel DNS. The computational box size is $6\pi h \times 2h \times 2\pi h$ for all flow cases. Flow cases INC7-INC10 are taken from the dataset of Bernardini et al. [15], whereas all other simulations have been performed in the present study.

computational arrangement of the DNS are given in table 1. For the sake of comparison, a set of incompressible channel DNS have been carried out so as to accurately reproduce the relevant friction Reynolds number for fair comparison of incompressible and compressible flow statistics (see the later discussion), whose details are reported in table 2. The numerical algorithm used for the incompressible DNS is the same as in previous studies from our group [15].

The compressible solver is first tested in the nearly incompressible regime ($M_b = 0.1$, corresponding to flow case CH01 of table 1), and compared with strictly incompressible data (flow case INC3 of table 2) in figure 2. Excellent agreement of the mean velocity and Reynolds stress distributions is recovered.

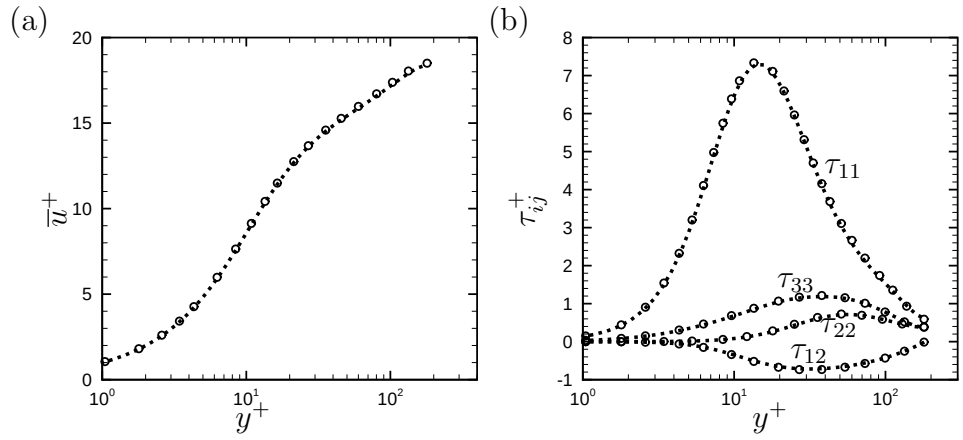

Figure 2: Performance in near-incompressible flow conditions: mean velocity profile (a) and Reynolds stresses (b) for flow case CH01 (circles) and INC3 (dots) (see tables 1 and 2).

The performance in the supersonic regime is tested by comparing our DNS data with reference data of Morinishi et al. [19], at $M_b = 1.5$, $Re_b = 6000$. Three DNS are presented in figure 3, one using the same set-up as all other DNS in terms of box size and resolution (CH15A), one in which the same box size and mesh resolution as Morinishi et al. [19] is used (labeled as CH15M), and one with same box size as Morinishi et al. [19], but improved resolution (labeled as CH15MF). Overall, very similar results are obtained for the various flow statistics, except for the peak of the streamwise Reynolds stress, which is known to be quite sensitive to mesh resolution. It appears that when using the same mesh resolution we very nearly match the results of Morinishi et al. [19]. However, refining the mesh has some impact on the Reynolds stress peak, which is underestimated by about 5% in the coarser computations. On the other hand, the effect of enlarging the computational box seems to be marginal at this modest Reynolds number.

3. Compressibility transformations

Several propositions have been made in the past to remove compressibility effects from statistics of wall-bounded flows, starting from analytical transformations of the laminar boundary layer equations [37]. In laminar boundary layer flow, the Howarth-Dorodnitsyn transformation exactly ac-

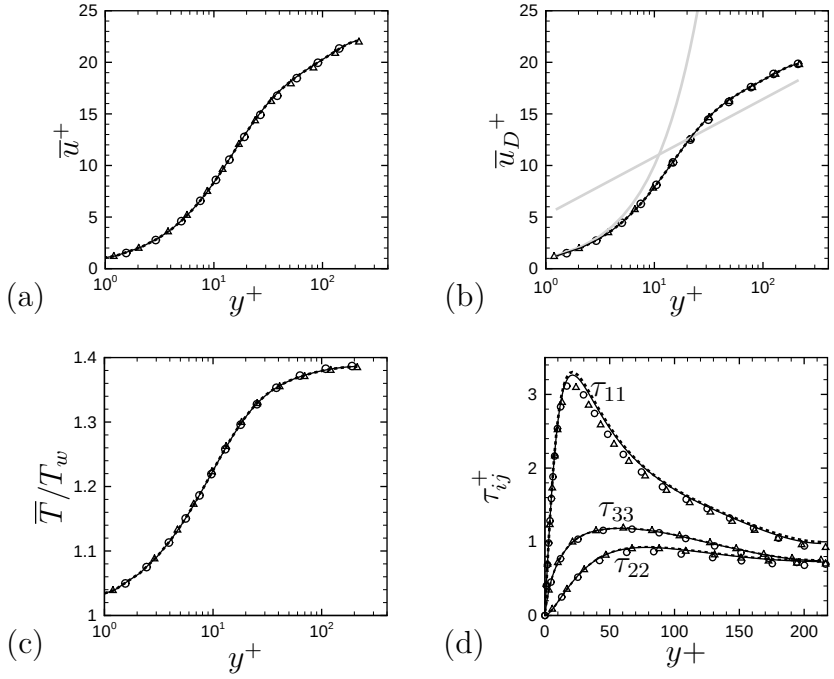

Figure 3: Comparison with DNS data of Morinishi et al. [19] (circles): mean velocity (a), van Driest-transformed velocity (b), mean temperature (c), and normal Reynolds stresses (d), for flow cases CH15A (solid), CH15M (triangles), CH15MF (dashed) (see table 1), The thick gray lines in panel (b) denote the compound law-of-the-wall $u^+ = y^+$, $u^+ = 5.2 + \log y^+/0.41$.

Transformation	Wall distance (f_I)	Mean velocity (g_I)	Stresses (φ_I)
Howarth [37]	$f_L = \frac{1}{N}$	$g_L = 1$	NA
Viscous sublayer	$f_V = 1$	$g_V = RN$	NA
van Driest [8]	$f_D = 1$	$g_D = R^{1/2}$	$\varphi_D = R$
Huang et al. [10]	$f_H = \frac{\mathrm{d}}{\mathrm{d}y}\left(\frac{y}{R^{1/2}N}\right)$	$g_H = R^{1/2}\left(1 + \frac{\tilde{u}}{R}\frac{\mathrm{d}R}{\mathrm{d}y}\frac{\mathrm{d}y}{\mathrm{d}\tilde{u}}\right)$	$\varphi_H = R$
Brun et al. [23]	$f_B = \frac{1}{RN}$	$g_B = \frac{1}{R^{1/2}N}\frac{y}{y_B}$	$\varphi_D = \frac{1}{RN^2}\left(\frac{y}{y_B}\right)^2$
Trettel and Larsson [1]	$f_T = \frac{\mathrm{d}}{\mathrm{d}y}\left(\frac{y}{R^{1/2}N}\right)$	$g_T = RN\frac{\mathrm{d}}{\mathrm{d}y}\left(\frac{y}{R^{1/2}N}\right)$	$\varphi_T = R$

Table 3: Transformation rules for wall distance, mean velocity and Reynolds stresses, according to equations (11), (22), with $N = \overline{\nu}/\nu_w$, $R = \overline{\rho}/\overline{\rho}_w$. **See equation 11 for the definition of the mapping functions f_I, g_I.**

counts for variations of mean density and temperature through re-scaling of the wall-normal coordinate thus reducing the transformed boundary layer equations to the incompressible ones. The same mapping does not directly apply to channel flow as the momentum equation is not homogeneous, reducing to

$$\frac{\mathrm{d}}{\mathrm{d}y}\left(\mu\frac{\mathrm{du}}{\mathrm{d}y}\right)+\frac{\tau_w}{h}=0. \tag{4}$$

A solution of equation (4) can be found by introducing an effective velocity

$$u_V=\int_0^u\frac{\mu}{\mu_w}\mathrm{d}u, \tag{5}$$

which satisfies the incompressible Poiseuille profile. The scenario is much more complicated in turbulent wall layers, in which no analytical transformation can be found to rigorously transform the governing equations to the incompressible ones. The only provable result pertains to the viscous sublayer, for which the mapping (5) still applies [5].

As regards the outer layer, the classical analysis is based on the work of van Driest [8]. Mean momentum balance in turbulent channel flow requires

$$\overline{\mu}\frac{\mathrm{d}\widetilde{u}}{\mathrm{d}y}-\overline{\rho}\widetilde{u''v''}=\overline{\rho}_w u_\tau^2\left(1-\eta\right), \tag{6}$$

where $\eta=y/h$ is the outer-scaled vertical coordinate. Away from the wall molecular viscosity is negligible, and further assuming $\eta<<1$, constancy of the turbulent stress follows, hence

$$-\widetilde{u''v''}\approx\left(\frac{\overline{\rho}_w}{\overline{\rho}}\right)u_\tau^2, \tag{7}$$

which shows that 'compressible' stresses should be scaled by the local mean density to recover the incompressible behavior. Mixing length modeling of the turbulent shear stress further leads to the classical overlap-layer equation

$$\frac{du_D}{dy}=\frac{u_\tau}{ky}, \tag{8}$$

in terms of the van Driest transformed velocity, defined as

$$u_D=\int_0^{\bar{u}}\left(\frac{\bar{\rho}}{\bar{\rho}_w}\right)^{1/2}\mathrm{d}\widetilde{u}. \tag{9}$$

Integration of (8) directly leads to a logarithmic layer for the transformed velocity field with the same slope as in the incompressible case, however with an additive constant which may in general vary with both Reynolds and Mach number. It should be noted that, assuming for simplicity a power-law expression for the molecular viscosity of the type $\mu \sim T^{0.76}$, it follows that the integrand of the viscous sublayer transformation (5) scales as $(\overline{\rho}_w/\overline{\rho})^{0.76}$, whereas in van Driest outer-layer transformation the scaling is about the inverse. Hence, it appears that van Driest transformation cannot collapse the entire wall layer, **except for the case of an adiabatic wall, since $\overline{\rho}/\overline{\rho}_w \approx 1$ in the near-wall region [12]. This condition is asymptotically approached in channel flows as $\boldsymbol{Re}_b \to \infty$, since the heat flux coefficients drops to zero (see table 1), hence it may be expected that the van Driest transformation recovers its accuracy in this limit.**

Failure of van Driest transformation was highlighted in previous works, in which alternative transformations were proposed to scale the whole inner layer. Empirical evidence [10] suggested that normalizing the mean velocity and Reynolds stress profiles with respect to suitable semi-local wall units based on the local density and viscosity, defined as

$$u_\tau^* = \sqrt{\tau_w/\overline{\rho}}, \quad \delta_v^* = \overline{\nu}/u_\tau^*, \tag{10}$$

yields better collapse of the flow statistics across the Mach number range. It can be readily shown [1] that using the local wall units defined in equation (10) is equivalent to introducing a mapping for the mean velocity and the wall distance, as given in equation 11 below. Brun et al. [23] pointed out the importance of accounting for mean viscosity variations in the presence of high Mach number and/or hot/cold walls. Using arguments strictly applicable to the viscous sublayer, those authors proposed a set of transformation rules which includes a wall-normal stretching similar to the Howarth-Dorodnitsyn transformation.

To gauge the validity of the various transformation rules, we preliminarily note that all of them can be cast in terms of mapping functions f_I, g_I for wall distance and mean velocity, defined as

$$y_I = \int_0^y f_I \, \mathrm{d}y, \quad u_I = \int_0^{\tilde{u}} g_I \, \mathrm{d}\tilde{u}, \tag{11}$$

where u_I and y_I denote the 'incompressible' values obtained from various transformations. Introducing these transformations into equation (6), and

assuming that the turbulent shear stress distribution obeys van Driest scaling, namely

$$-\overline{\rho}\widetilde{u''v''} = \overline{\rho}_w \tau_I(y_I), \tag{12}$$

we find

$$\frac{\overline{\mu}}{\mu_w}\frac{f_I}{g_I}\frac{\mathrm{d}u_I^+}{\mathrm{d}y_I^+} + \tau_I^+ = (1-\eta)\,. \tag{13}$$

Comparing equation (13) with its incompressible counterpart then directly yields

$$\frac{\overline{\mu}}{\mu_w}\frac{f_I}{g_I} = 1, \tag{14}$$

which may be regarded as a constraint which defines a class of compressibility transformations which satisfy universality of the turbulent stresses.

The mapping functions for wall distance and mean velocity corresponding to various compressibility transformations are listed in table 3. Of course, the only **exhisting** transformation which satisfies the constraint given by equation (14) is that for the viscous sublayer. A **novel** velocity transformation which also satisfies (14), with the additional constraint that the transformed velocity profile collapses to the universal incompressible profile in the overlap layer, has been recently derived by Trettel and Larsson [1], and it is also listed in table 3. It is interesting to note that the transformation rule for the wall-normal distance is identical to Huang's transformation (hence $y_T = y_H$).

An important issue related to compressibility transformations is the definition of a suitable Reynolds number to compare the flow statistics across Mach numbers and with incompressible data. For instance, Coleman et al. [17] compared compressible channel statistics with the incompressible DNS of Kim et al. [13] at approximately the same friction Reynolds number, whereas Morinishi et al. [19] used a friction Reynolds number defined with the local viscous length scale at the channel centerline. We argue that the answer to the 'most relevant' Reynolds number should be given a-posteriori, based on the most successful transformation. For that purpose, we define a friction Reynolds number for the generic transformation as the ratio of the transformed wall-normal coordinate at the channel centerline to the viscous length scale evaluated at the wall, hence

$$Re_{\tau I} = y_I(h)/\delta_v, \tag{15}$$

which clearly reduces to the conventional definition in the incompressible limit. In the following, in an attempt to evaluate the various compressibil-

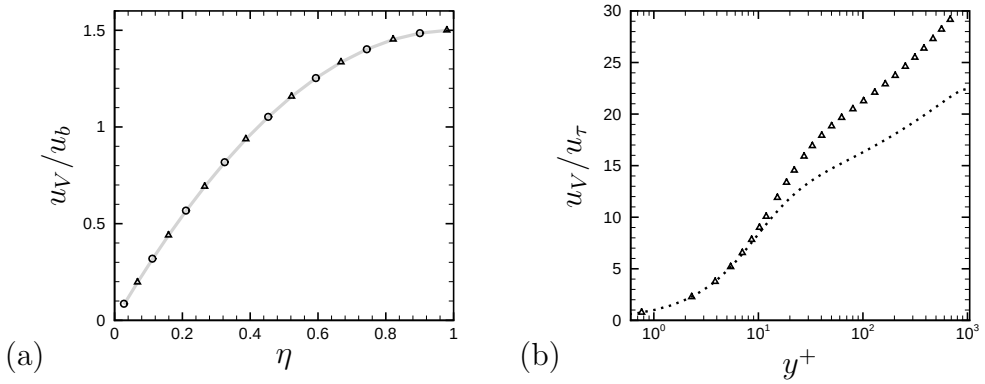

Figure 4: Assessment of laminar scaling, as from equation (5): (a) laminar flow at $M_b = 1.5$ (triangles) and $M_b = 3$ (circles), compared with the parabolic Poiseuille profile (gray solid line); (b) comparison of flow case CH15C (triangles) with INC10 (dotted lines).

ity transformations as fairly as possible, we compare the inner-scaled transformed distributions of the velocity statistics with incompressible DNS data at exactly the same relevant friction Reynolds number.

3.1. Mean velocity

As a preliminary check, in figure 4a we evaluate the viscous sublayer transformation given in equation (5) for the case of compressible laminar flow at $M_b = 1.5$ and $M_b = 3$. It is clear that equation (5) effectively maps the compressible velocity profiles to the incompressible parabolic Poiseuille distribution. Figure 4b further shows equation (5) applied to flow case CH15C. In this case, satisfactory collapse to the incompressible distribution is recovered in the viscous sublayer up to $y^+ \approx 10$, with obvious deviations farther from the wall.

The inner-scaled velocity distributions obtained from application of the compressibility transformations listed in table 3 are compared in figures 5-8 with incompressible DNS data at the same relevant friction Reynolds number. For reference, the alleged universal incompressible wall law is also shown. As also found in previous studies [17, 5], the van Driest transformation (figure 5) visibly undershoots the viscous sublayer linear distribution, especially in flow case CH3, and it overshoots the incompressible velocity distribution away from the wall, the crossing occurring at $y^+ \approx 30$. The van Driest transformation yields the correct slope of the log law in the overlap layer, but

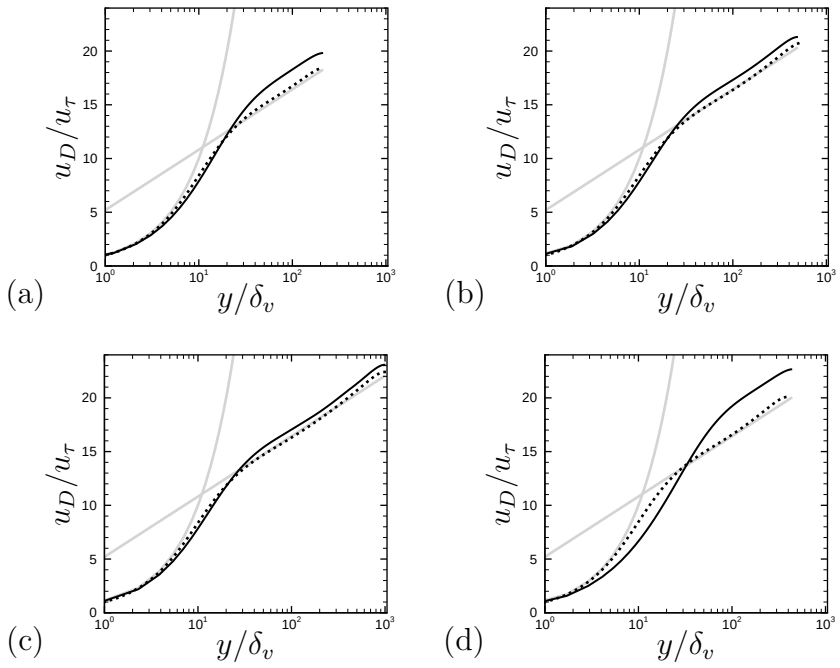

Figure 5: Mean velocity profiles transformed according to van Driest [8] (solid lines) for flow cases CH15A (a), CH15B (b), CH15C (c), CH3 (d), compared with incompressible DNS at matching $Re_{\tau D}$ (INC4, INC7, INC10, INC6, respectively, plotted with dotted lines). The thick gray lines denote the compound law-of-the-wall $u^+ = y^+$, $u^+ = 5.2 + \log y^+/0.41$.

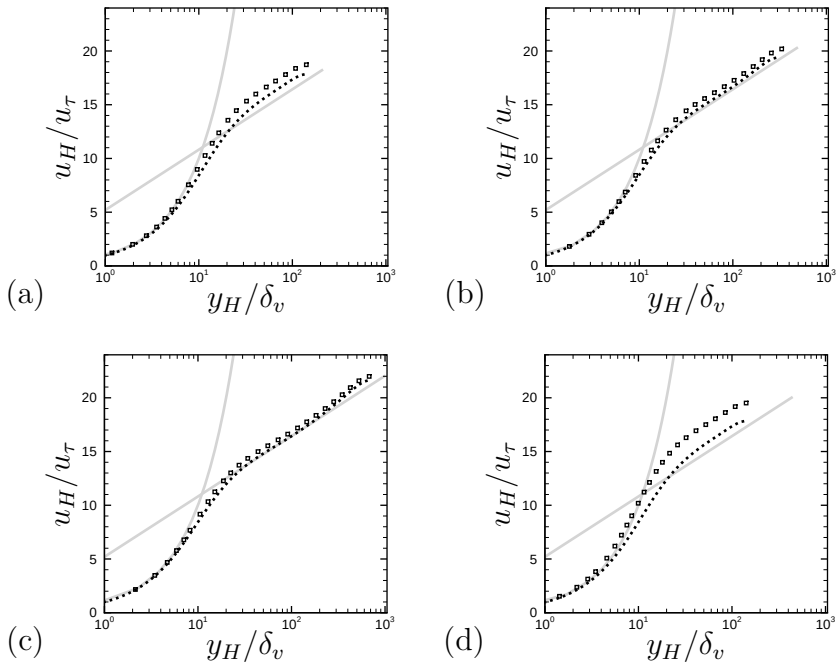

Figure 6: Mean velocity profiles transformed according to Huang et al. [10] (squares) for flow cases CH15A (a), CH15B (b), CH15C (c), CH3 (d), compared with incompressible DNS at matching $Re_{\tau H}$ (INC1, INC5, INC8, INC1, respectively, plotted with dotted lines). The thick gray lines denote the compound law-of-the-wall $u^+ = y^+$, $u^+ = 5.2 + \log y^+/0.41$.

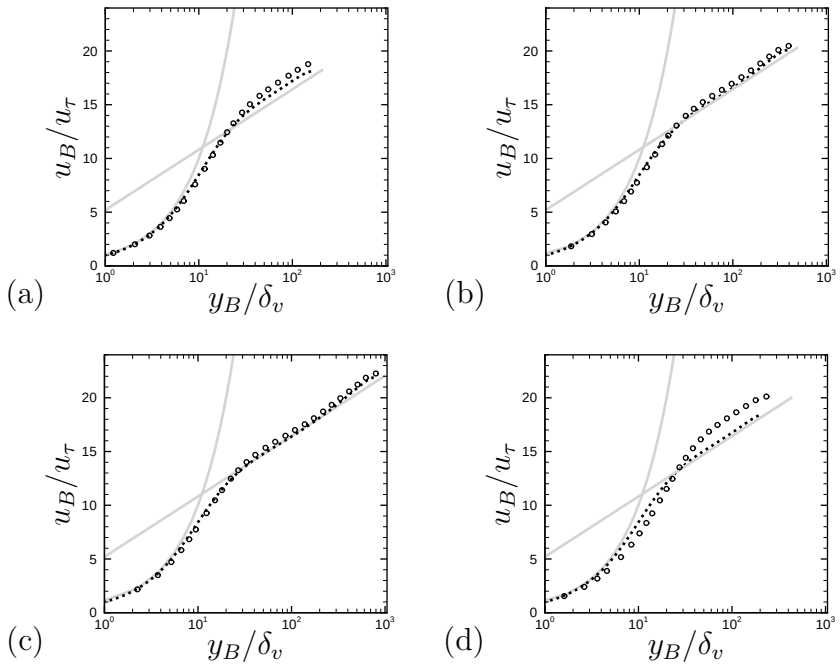

Figure 7: Mean velocity profiles transformed according to Brun et al. [23] (circles) for flow cases CH15A (a), CH15B (b), CH15C (c), CH3 (d), compared with incompressible DNS at matching $Re_{\tau B}$ (INC2, INC6, INC9, INC4, respectively, plotted with dotted lines). The thick gray lines denote the compound law-of-the-wall $u^+ = y^+$, $u^+ = 5.2 + \log y^+/0.41$.

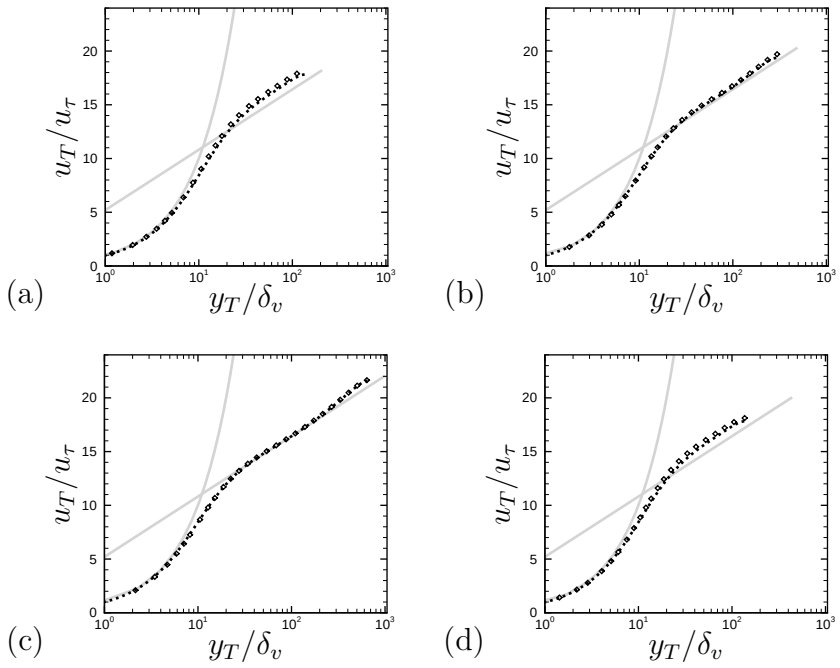

Figure 8: Mean velocity profiles transformed according to Trettel and Larsson [1] (diamonds) for flow cases CH15A (a), CH15B (b), CH15C (c), CH3 (d), compared with incompressible DNS at matching $Re_{\tau T}$ (INC1, INC5, INC8, INC1, respectively, plotted with dotted lines). The thick gray lines denote the compound law-of-the-wall $u^+ = y^+$, $u^+ = 5.2 + \log y^+/0.41$.

the additive constant is significantly overestimated at low Reynolds number, whereas it approaches the incompressible value at sufficiently high Reynolds number, as also noticed by Huang and Coleman [38], Fernholz and Finley [39], Spina et al. [31], and as probably due to the reduction in the heat flux coefficient (see table 1).

Unlike van Driest, Huang's transformation, shown in figure 6, performs well in the near-wall region, whereas it systematically overshoots the incompressible velocity profile in the outer layer, again approaching the incompressible behavior at sufficiently high Reynolds number. Brun's transformation (see figure 7) has an overall similar behavior as van Driest transformation, although absolute deviations in the outer layer are significantly smaller. The limitations of earlier transformations are apparently overcome by the transformation by Trettel and Larsson [1] (see figure 8), which yields collapse to the incompressible distributions across the Reynolds and Mach number range, throughout the wall layer.

Closer scrutiny of the core part of the flow can be gained by inspecting the mean velocity profiles in defect form, as given in figure 9. A parabolic law for the core velocity profile of incompressible channels has recently been derived by Pirozzoli [40]. The derivation stems from the idea that the outer-layer turbulent eddies are not directly affected by the presence of the wall, and their size should hence scale with the channel height and with the typical eddy velocity scale (namely the friction velocity), whence it follows that the relevant eddy viscosity is

$$\nu_t = c_\mu u_\tau h, \tag{16}$$

where c_μ a suitable constant. This reasoning is easily extended to compressible flows on the token that in the presence of mean density variations the effective velocity scale is u_τ^* (as defined in equation (10)) rather than u_τ, which yields the eddy viscosity

$$\nu_t = c_\mu^* u_\tau^* h, \tag{17}$$

where c_μ^* might differ from c_μ owing to compressibility effects. From equation (6), neglecting the viscous term and using the eddy viscosity (17), one readily obtains

$$\frac{\mathrm{d}\widetilde{u}^+}{\mathrm{d}\eta} = \frac{1}{c_\mu^*}\left(\frac{\overline{\rho}_w}{\bar{\rho}}\right)^{1/2}(1-\eta)\,, \tag{18}$$

from which it follows that the van-Driest-transformed velocity should follow

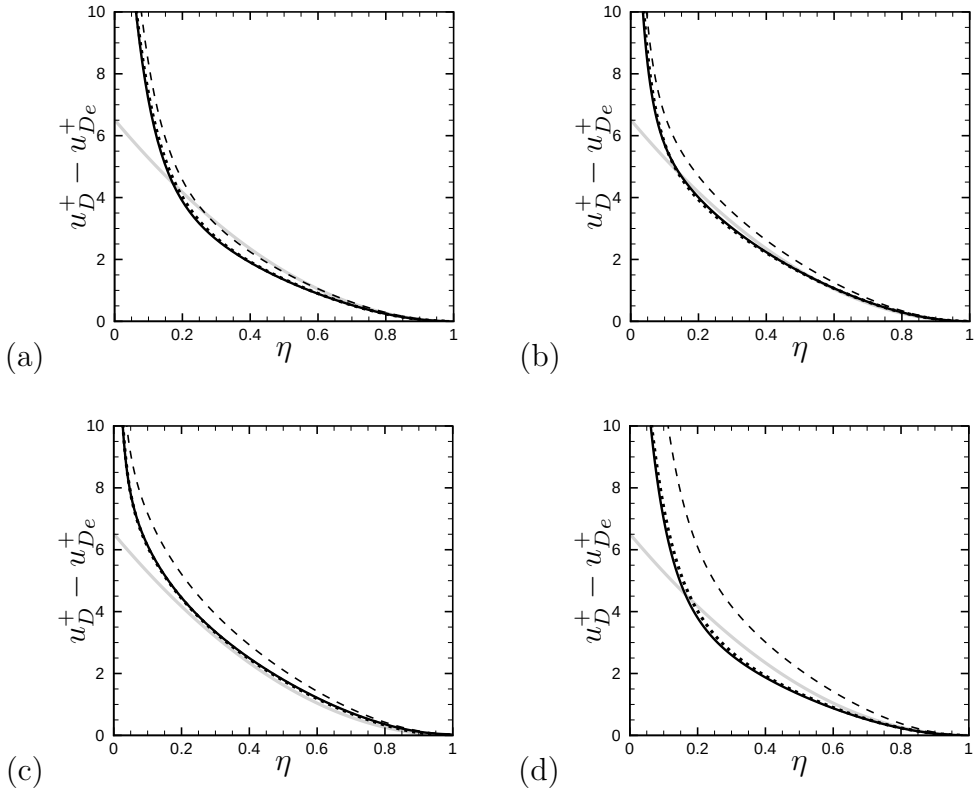

Figure 9: Van Driest-transformed defect velocity profiles for flow cases CH15A (a), CH15B (b), CH15C (c), CH3(d) (solid lines), compared with incompressible data from flow cases INC1-INC5-INC8-INC1 (dotted lines), at matching $Re_{\tau H}$. The dashed lines represent the untransformed velocity profiles. The 'e' subscript refers to properties at the channel centerline. The gray line represent equation (18) with $c_\mu = 0.0767$.

a universal parabolic law in the core part of the channel

$$u_D^+ - u_{De}^+ = -\frac{1}{2c_\mu^*}\left(1-\eta\right)^2, \tag{19}$$

where u_{De} is the transformed centerline velocity.

Outer defect profiles obtained with van Driest transformation are given in figure 9, the other transformations yielding similar results, since density and viscosity variations in the outer layer are but moderate. Comparison with incompressible DNS (dotted lines) shows excellent agreement throughout the outer layer, irrespective of the Reynolds and Mach number. The DNS data are consistent with the prediction of equation (19) around the channel centerline, the range of validity of the parabolic fit extending to about half of the flow domain at sufficiently high Reynolds number. No evident compressibility effects are observed on the parabolic law constant, which in fact coincides with its incompressible value.

3.2. Reynolds stresses and vorticity fluctuations

Here we discuss the validity of compressibility transformations as applied to the individual components of the Reynolds stress tensor, for which direct extension of the van Driest scaling yields

$$\tau_{Dij} = \frac{\overline{\rho}}{\overline{\rho}_w}\tau_{ij}. \tag{20}$$

The same assumption also subtends the scalings of Huang et al. [10] and Trettel and Larsson [1]. A different form of scaling was considered by Brun et al. [23], who applied the same scaling factor used for the mean velocity to scale the turbulence velocity intensities, thus yielding

$$\tau_{Bii} = \frac{\overline{\rho}}{\overline{\rho}_w}\left(\frac{y}{y_B}\frac{\mu_w}{\overline{\mu}}\right)^2\tau_{ii}, \tag{21}$$

for the diagonal Reynolds stress components. The scaling rules for the Reynolds stresses are summarized in table 3, in the form of the ratio of the transformed to the untransformed stresses, namely

$$\varphi_I = \frac{\tau_I}{\tau}. \tag{22}$$

Figure 10 shows the van Driest-transformed Reynold stress components, compared with the corresponding incompressible distributions. As noticed

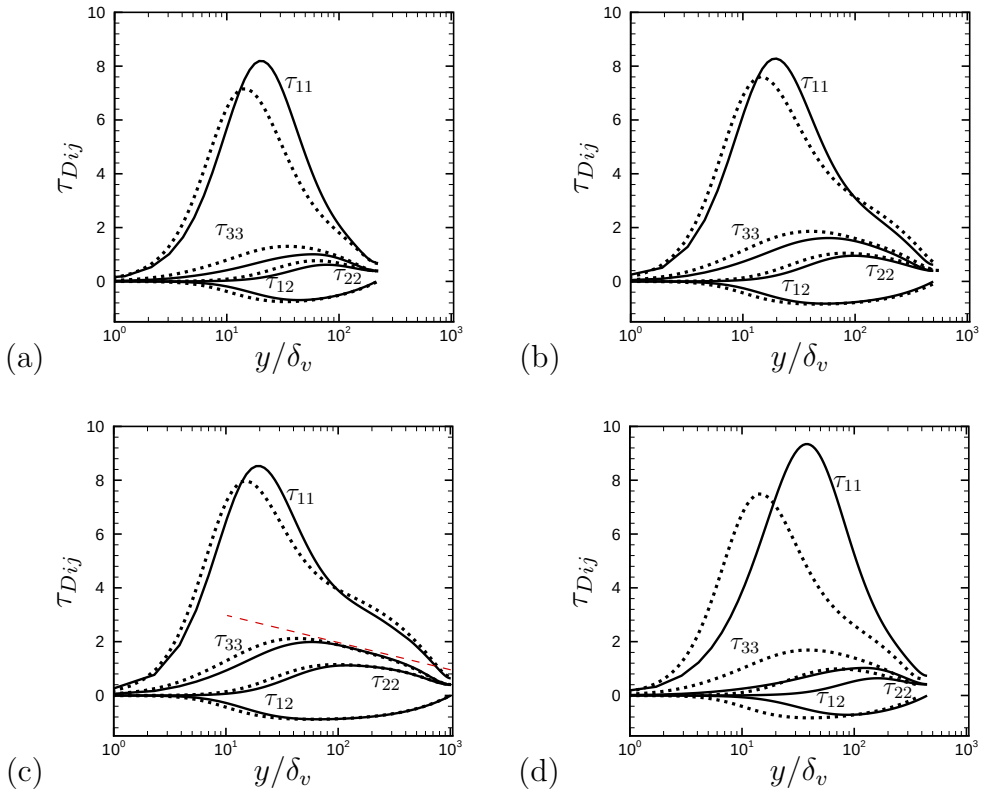

Figure 10: Reynolds stress components transformed according to van Driest [8] (solid lines) for flow cases CH15A (a), CH15B (b), CH15C (c), CH3 (d), and compared with incompressible DNS at matching $Re_{\tau D}$ (INC4, INC7, INC10, INC6, respectively, with dotted lines). The dashed line in panel (c) denotes a logarithmic fit of the data.

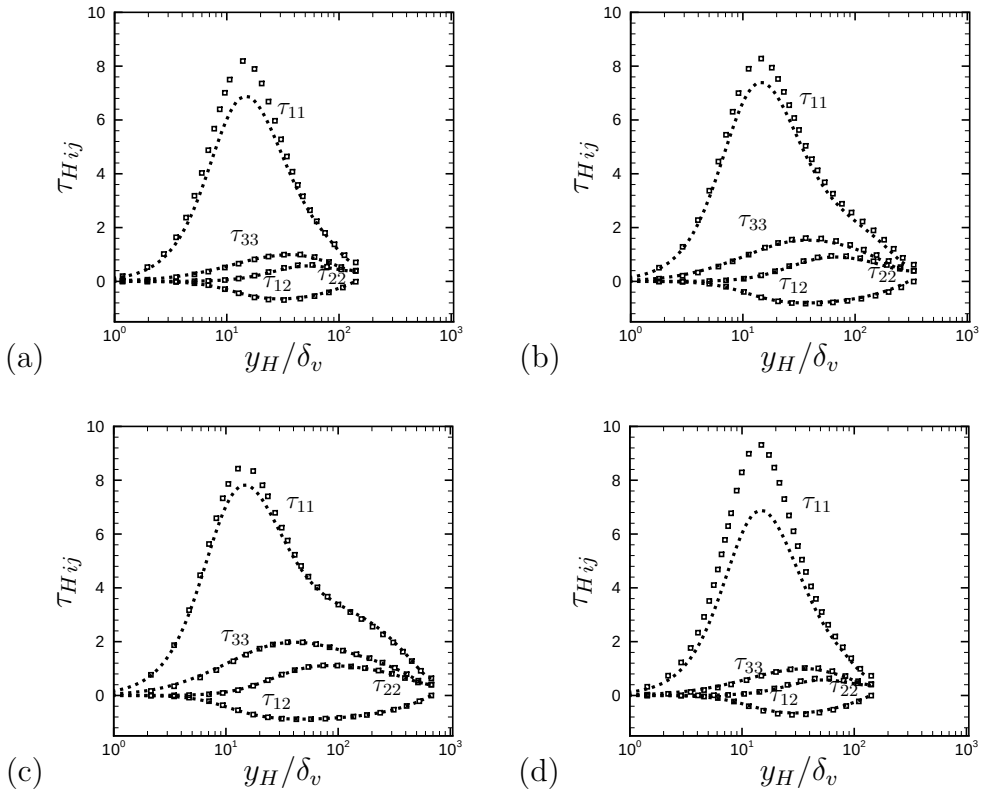

Figure 11: Reynolds stress components transformed according to Huang et al. [10] (squares) for flow cases CH15A (a), CH15B (b), CH15C (c), CH3 (d), compared with incompressible DNS at matching $Re_{\tau H}$ (INC1, INC5, INC8, INC1, respectively, with dotted lines).

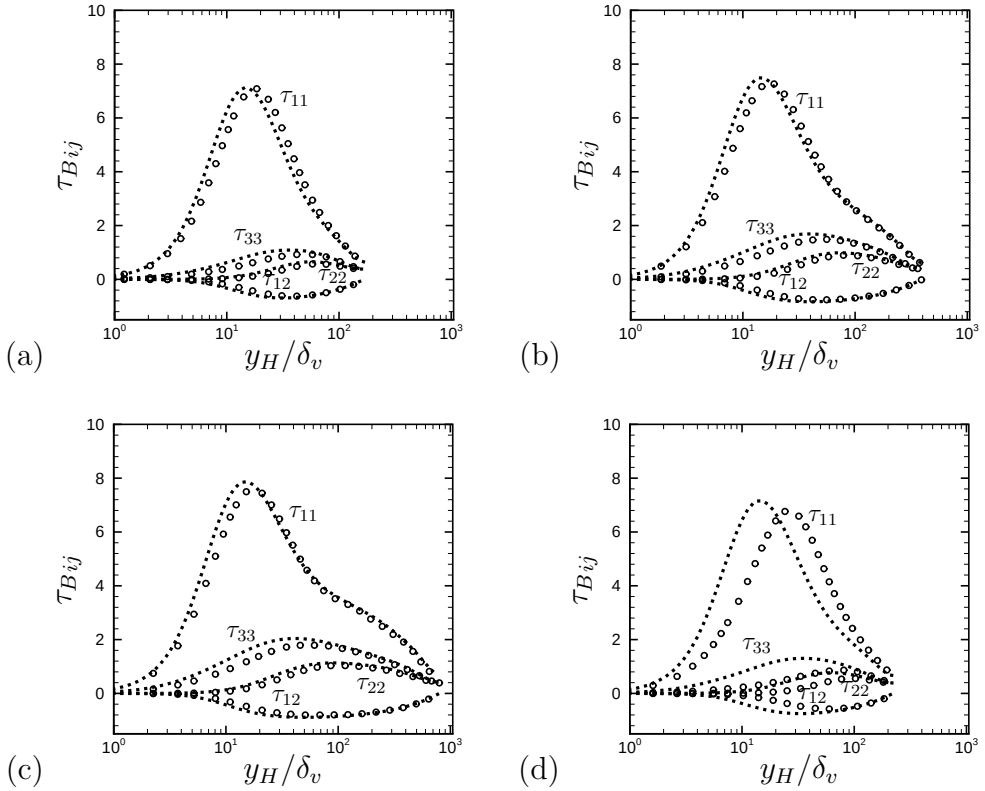

Figure 12: Reynolds stress components transformed according to Brun et al. [23] (circles) for flow cases CH15A (a), CH15B (b), CH15C (c), CH3 (d), compared with incompressible DNS at matching $Re_{\tau B}$ (INC2, INC6, INC9, INC4, respectively, with dotted lines).

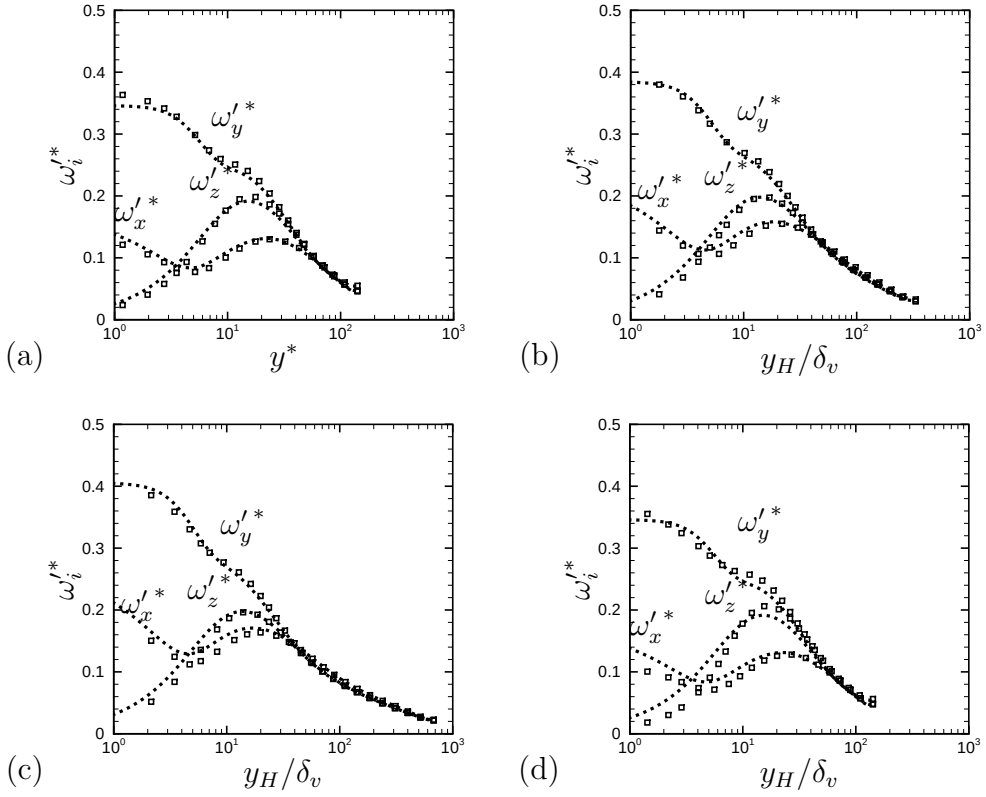

Figure 13: Vorticity fluctuations in semi-local scaling, $\omega_i'^* = \omega_i'\delta_v^*/u_\tau^*$ (squares) for flow case CH15A (a) CH15B (b) CH15C (c), CH3 (d), compared with incompressible DNS at matching $Re_{\tau H}$ (INC1, INC5, INC8, INC1, respectively, with dotted lines).

in previous studies [17, 22], a mismatch between scaled compressible stresses and incompressible stresses is found in the inner layer, with clear difference in the amplitude of the streamwise stress and a shift in the position of peaks, whereas closer agreement is found in the outer layer. It is noteworthy that the in flow case CH15C (see panel c) a substantial layer with near-logarithmic variation of the spanwise stress is recovered [41], which is the symptom of the emergence of effects of scale separation, not attained in previous studies at lower Reynolds number. Figure 11 shows that Huang's scaling yields much better collapse of the compressible and incompressible stresses distributions, in terms of both the peak amplitude and the off-wall position. In fact, the shear stress and the wall-normal and spanwise velocity variances are almost perfectly matched, whereas differences remain for the amplitude of the streamwise turbulence intensity peak. Superior accuracy of Huang's scaling as compared to van Driest was also observed in previous studies [17, 19], but to our knowledge this is the first time that a comparison is carried out at precisely matching Reynolds number. Brun's scaling is tested for the Reynolds stress tensor components in figure 12. Note that, although the transformation (21) was originally meant for the normal stresses only, we also apply it to the shear stress. The transformed stresses shows reasonably good collapse on the incompressible simulations in the outer layer for flow cases CH15A-B-C, but they are less accurate in the near-wall region, similar to what observed for the van Driest transformation. As the Mach number is increased (panel d) Brun's transformation appears to fail both in the inner and in the outer layer. Interestingly, Brun's transformation seems to yield good prediction of the amplitude of the streamwise stress peak, although its positions is clearly shifted with respect to the 'correct' one. Trettel's transformation for the Reynolds stresses is not shown here, being identical to Huang's.

The vorticity fluctuation components are presented in figure 13, scaled in semi-local units, as defined in equation (10). The success in collapsing the various distributions is particularly impressive here, except perhaps for minor differences in the near-wall region for flow case CH3. This observation probably points to the physical fact that the small scales of fluid motion only depend on the local mean flow conditions, in terms of density and viscosity.

4. Mean temperature

The distribution of the mean temperature is of great importance in compressible boundary layers, as it obviously allows prediction of the heat trans-

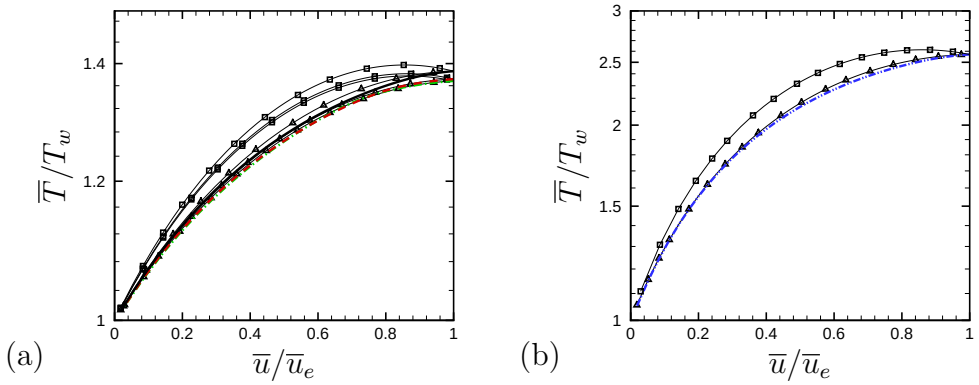

Figure 14: Temperature-velocity relationship: mean temperature as a function of mean velocity. In panel (a) flow cases CH15A (black, solid) -CH15B (red, dashed)-CH15C (green, dash-dotted), in panel (b) flow case CH3 (blue, dash-dot-dot) compared with equation (23) (solid lines with square symbols) and with (24) (solid lines with triangle symbols), with $r = 0.89$.

fer coefficient, but it is also necessary for accurate prediction of the skin friction coefficient, as an accurate temperature-velocity relation allows straightforward application of the inverse of the compressibility transformations of table 3 to determine the mean velocity profile in untransformed space [39]. A widely used temperature-velocity relationship was derived by Walz [27],

$$\frac{T}{T_w} = 1 + \frac{T_r - T_w}{T_w}\frac{\overline{u}}{\overline{u}_e} - r\frac{\gamma - 1}{2}M_e^2\frac{T_e}{T_w}\left(\frac{\overline{u}}{\overline{u}_e}\right)^2, \tag{23}$$

where $T_r = T_e\left(1 + \frac{\gamma-1}{2}rM_e^2\right)$ is the recovery temperature, $r = 0.89$ is the recovery factor, and the subscript e denotes properties at the edge of the wall layer (the channel centerline in internal flow). Walz obtained equation (23) from a simplified form of the energy equation [8, 42], based on several assumptions including neglect of turbulent dissipation and pressure-strain terms. Pirozzoli et al. [43] found good agreement between equation (23) and DNS of a $M = 2.25$ boundary layer over an adiabatic wall. Duan et al. [28] carried out DNS of a supersonic boundary layer at $M = 5$ with different wall temperatures, finding good agreement between equation (23) in adiabatic wall cases, but differences as the wall heat flux increases. Recently, Zhang et al. [3] derived a generalized Reynolds analogy by introducing a general recovery factor, which overcomes the limitations of Walz equation in the

presence of non-adiabatic walls

$$\frac{T}{T_w} = 1 + \frac{T_{rg} - T_w}{T_w}\frac{u}{u_e} + \frac{T_e - T_{rg}}{T_w}\left(\frac{u}{u_e}\right)^2, \tag{24}$$

where $T_{rg} = T_e + r_g u_e^2/(2C_p)$, $r_g = 2C_p(T_w - T_e)/u_e^2 - 2Prq_w/(u_e\tau_w)$. Equation (24) explicitly takes into account the wall heat flux q_w, and it coincides with Walz relation in the case of adiabatic walls.

Figure 14 provides a comparison between the channel flow DNS data and the predictions of equation (23) and (24), which clearly shows superior performance of the latter, especially at higher Mach number. It is worth pointing out that equations (23)-(24) have the same form for external and internal flows, but in the latter case the centerline values of temperature and velocity are not known a priori. As a consequence, these traditional temperature/velocity relations cannot be used to explicitly determine the friction coefficient, and their engineering relevance in this case is more limited than in boundary layers.

5. Length scales

We now focus on the evaluation of the typical length scales in the outer wall layer. As far as theory goes, the basic prediction of the attached eddy model for incompressible wall layers [44, 45], is that the typical length scales should increase linearly with the wall distance in the outer layer, which is consistent with the existence of a logarithmic layer in the mean velocity profile. A more refined assumption [46] is that the outer-layer length scales should scale with the local mean shear, as follows

$$\ell_m \sim u_\tau \left(\frac{\mathrm{d}\overline{u}}{\mathrm{d}y}\right)^{-1}, \tag{25}$$

which in fact predicts linear variation in the presence of a logarithmic mean velocity profile. A simple eddy-viscosity ansatz led Pirozzoli [47] to predict a rather different scaling,

$$\ell_{12} \sim (u_\tau h)^{1/2} \left(\frac{\mathrm{d}\overline{u}}{\mathrm{d}y}\right)^{-1/2}, \tag{26}$$

which was shown to apply with greater accuracy than (25) far from the wall. The scaling (26) can be readily adapted to compressible flow on the token

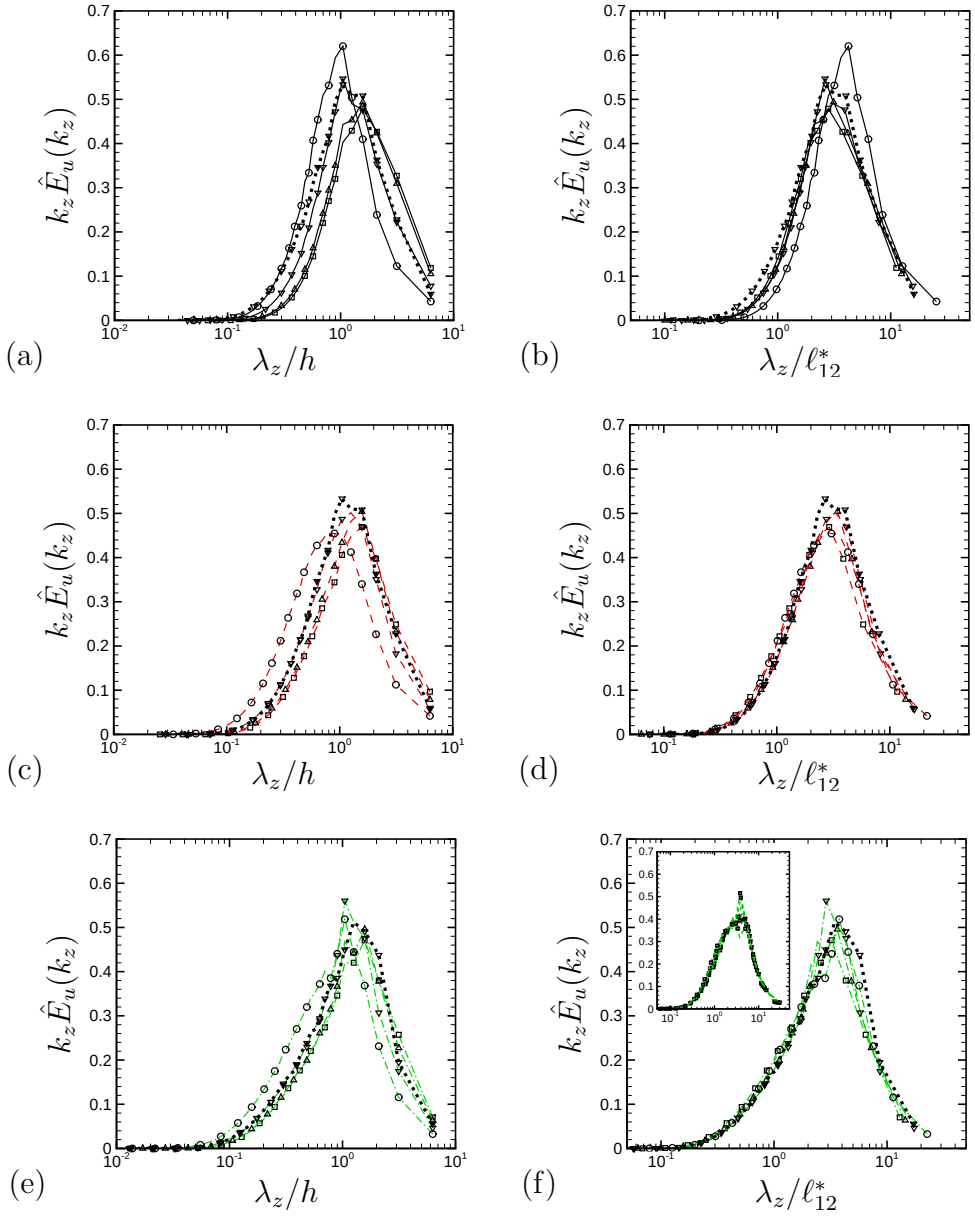

Figure 15: Pre-multiplied power spectral densities of u in spanwise direction as a function of λ_z/h (a-c-e) and λ_z/ℓ^*_{12} (b-d-f), for flow cases CH15A (a-b), CH15B (c-d), CH15C (e-f). Symbols denote different distances from the wall, namely $\eta = 0.2$ (circles), $\eta = 0.4$ (gradients), $\eta = 0.6$ (deltas), $\eta = 0.7$ (squares). The dotted lines with gradient symbols denotes the incompressible spectrum at $\eta = 0.4$ at matching $Re_{\tau H}$. The inset in panel (f) shows the spectra of CH15C at six stations in the logarithmic region between $y^+_H = 100$ and $y^+_H = 200$.

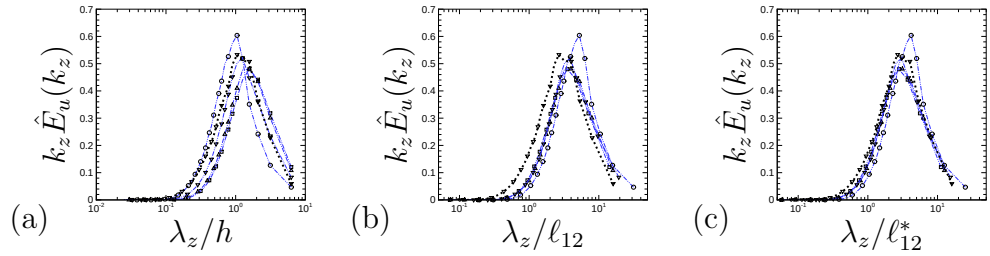

Figure 16: Pre-multiplied spectral densities in spanwise direction for the streamwise velocity component, as a function of λ_z/h (a), λ_z/ℓ_{12} (b) and λ_z/ℓ^*_{12} (c) for flow case CH3. Symbols denote different distances from the wall, namely $\eta = 0.2$ (circles), $\eta = 0.4$ (gradients), $\eta = 0.6$ (deltas), $\eta = 0.7$ (squares). The dotted lines with gradient symbols denotes the incompressible spectrum at $\eta = 0.4$ at matching $Re_{\tau H}$.

that the main compressibility effects are included in the variation of the local friction velocity, with the following result

$$\ell^*_{12} \sim (u^*_\tau h)^{1/2} \left(\frac{\mathrm{d}\tilde{u}}{\mathrm{d}y} \right)^{-1/2}. \tag{27}$$

In order to gauge the accuracy of the scaling given in equation (27), we will focus on the spanwise spectral densities of u, defined such that

$$\widetilde{u''^2} = \int_0^\infty E_u(k_z)\, dk_z, \tag{28}$$

where k_z is the Fourier wavenumber in the spanwise direction. This choice is motivated by the peculiar streaky pattern of the wall layer 'superstructures', which are relatively compact in the spanwise direction, whereas they are essentially infinite in the streamwise direction, and estimation of the actual length scale based on streamwise two-point correlations or one-dimensional spectra is prone to large uncertainties [48]. To account for the effect of turbulence intensity variation across the wall layer, we further consider the normalized spectral densities, defined as

$$\hat{E}_u(k_z) = E_u(k_z)/\widetilde{u''^2}. \tag{29}$$

Figure 15 shows the spectra of u in pre-multiplied form, as a function of the spanwise wavelength $\lambda_z = 2\pi/k_z$, normalized with respect to either h or ℓ^*_{12}. The spectra at different stations, all laying in the outer layer $50/Re_{\tau H} \leq$

$\eta \leq 0.7$, are shown and compared with the spectra from incompressible simulations at matching $Re_{\tau H}$, at $\eta = 0.4$. The outer-scaled spectra all show a distinct bump shape with peak at $\lambda_z \approx h$, which is suggestive of eddies having a typical spanwise size of the order of the channel half-height, and increasing with the wall distance. When reported in terms of the length scale (27), spectra at all off-wall locations are found to collapse on another as well as on the incompressible spectra, with greater scatter in the low-Re flow case (CH15A), in which the lowest location is at the very lower edge of the outer layer. It is worth noting that this scaling also applies to the overlap region (albeit small in this case), as seen in the inset of figure 15e. Compressibility effects are further scrutinized in figure 16, which pertains to flow case CH3. In this case, wavelengths are scaled with respect to h (a), ℓ_{12} (b), and ℓ^*_{12} (c). Comparison of panels (b) and (c) clearly shows superior accuracy of the heuristic compressibility correction given in equation (27), as compared to the baseline 'incompressible' scaling of equation (26).

Overall, we believe that the data presented above convincingly support the validity of the theory developed by Pirozzoli [47], from which more general conclusions can be drawn. Using the identity $u^*_\tau = u_\tau \sqrt{\rho_w/\rho}$, and using van Driest transformation for the mean velocity, which as previously seen is quite accurate in the outer wall layer, equation (27) becomes

$$\ell^*_{12}(y) \sim (u_\tau h)^{1/2} \left(\frac{\mathrm{d}u_D}{\mathrm{d}y} \right)^{-1/2}, \tag{30}$$

which coincides with the conventional length scale (26), applied to the transformed mean velocity profile. Since in the outer layer the transformed mean shear is the same at the same outer wall distance η, it follows that the typical spanwise length scales are not affected by compressibility. This is consistent with the previous figures 15, 16, which showed collapse with incompressible spectra and nearly identical distributions for flow cases CH15A and CH3 having very similar effective friction Reynolds number, and with previous experimental and DNS findings [33, 12].

6. Conclusions

We have presented results of a new DNS dataset of compressible channel flow at unprecedented Reynolds number, which allow to shed some additional light on the structure of compressible turbulent wall layers. Importantly,

compressible channel data are directly compared with incompressible channel DNS data at precisely matching Reynolds number. As far as 'compressibility transformations' are concerned, we find classical van Driest scaling to be inaccurate in representing the full inner-layer velocity profile, especially in the presence of significant wall heat flux. Later transformations, including Huang's and Brun's yield some improvement, especially because they more faithfully reproduce the correct behavior in the inner layer. It appears that a recent transformation by Trettel and Larsson [1] very well reproduces the behavior of the full mean velocity profile, with the side consequence that fair comparison of inner-scaled velocity profiles across the Mach number range should be carried out at matching friction Reynolds number based on y_H as defined in equation (11) + table 3. Huang's (and consequently Trettel's) transformation well performs for all Reynolds stress components, with the partial exception of the peak of the streamwise turbulent stress, which as seen in many previous studies [11]-[25] is higher than in the incompressible case. Reasons for this remaining discrepancy may constitute an interesting topic for future research. The outer-scaled mean velocity profile is reasonably well represented by all compressibility transformations, as density and viscosity variations are small. In particular, it is found that a parabolic profile well represents a substantial fraction of the wall layer, up to 50% at sufficiently high Reynolds number, which is characterized by a single, universal constant. Study of the mean velocity/temperature relation shows a classical quadratic dependence, however with different coefficients than the classical Walz formula, and which explicitly depend of the wall heat flux [3]. Put all together, the above findings may constitute the basis for the development of explicit approximations for the friction and heat flux coefficients in compressible turbulent channels, which are currently lacking. Finally, we have scrutinized the behavior of the length scales associated with the streamwise velocity field, for which no consensus exists at present. Limiting ourselves to the spanwise length scales, for which no ambiguity in the interpretation exists, we find that their dependence on wall distance, Reynolds and Mach number is well synthesized in formula (27), which is rooted in crude mixing length arguments. The direct consequence is that, for fixed Reynolds number and fixed wall distance, the length scales of the typical eddies should not vary with the Mach number. Further studies, especially at higher Mach number, would be desirable to further put this proposition to test.

Acknowledgements

We acknowledge that most of the results reported in this paper have been achieved using the PRACE Research Infrastructure resource FERMI based at CINECA, Casalecchio di Reno, Italy.

References

[1] A. Trettel, J. Larsson, Effect of cooling on compressible wall-turbulence, in: 67th Annu. Meet. APS Div. Fluid Dyn., volume 59 of *Bull. Am. Phys. Soc.*, 2014. URL: `http://meetings.aps.org/link/BAPS.2014.DFD.L26.5`.

[2] A. Trettel, J. Larsson, Mean velocity scaling for compressible wall turbulence with heat transfer, Phys. Fluids (2016). In preparation.

[3] Y. Zhang, W. Bi, F. Hussain, Z. She, A generalized Reynolds analogy for compressible wall-bounded turbulent flows, J. Fluid Mech. 739 (2014) 392–420.

[4] P. Bradshaw, Compressible turbulent shear layers, Annu. Rev. Fluid Mech. 9 (1977) 33–52.

[5] A. Smits, J.-P. Dussauge, Turbulent shear layers in supersonic flow, 2nd edn, American Istitute of Physics, 1996.

[6] T. Gatski, J.-P. Bonnet, Compressibility, turbulence and high speed flow, Academic Press, 2013.

[7] M. Morkovin, Effects of compressibility on turbulent flows, in: Mécanique de la Turbulence, A. Favre, 1962, pp. 367–380.

[8] E. van Driest, Turbulent boundary layer in compressible fluids, J. Aero. Sci. 18 (1951) 145–160.

[9] J. Gaviglio, Reynolds analogies and experimental study of heat transfer in the supersonic boundary layer, Intl J. Heat Mass Transfer 30 (1987) 911–926.

[10] P. Huang, G. Coleman, P. Bradshaw, Compressible turbulent channel flows: DNS results and modeling, J. Fluid Mech. 305 (1995) 185–218.

[11] S. Guarini, R. Moser, K. Shariff, A. Wray, Direct numerical simulation of a supersonic turbulent boundary layer at Mach 2.5, J. Fluid Mech. 414 (2000) 1–33.

[12] S. Pirozzoli, M. Bernardini, Turbulence in supersonic boundary layers at moderate Reynolds number, J. Fluid Mech. 688 (2011) 120–168.

[13] J. Kim, P. Moin, R. Moser, Turbulence statistics in fully developed channel flow at low Reynolds number, J. Fluid Mech. 177 (1987) 133–166.

[14] S. Hoyas, J. Jiménez, Scaling of the velocity fluctuations in turbulent channels up to $\mathrm{Re}_\tau = 2003$, Phys. Fluids 18 (2006) 011702.

[15] M. Bernardini, S. Pirozzoli, P. Orlandi, Velocity statistics in turbulent channel flow up to $\mathrm{Re}_\tau = 4000$, J. Fluid Mech. 742 (2014) 171–191.

[16] M. Lee, R. Moser, Direct simulation of turbulent channel flow layer up to $\mathrm{Re}_\tau = 5200$, J. Fluid Mech. 774 (2015) 395–415.

[17] G. Coleman, J. Kim, R. Moser, A numerical study of turbulent supersonic isothermal-wall channel flow, J. Fluid Mech. 305 (1995) 159–183.

[18] R. Lechner, J. Sesterhenn, R. Friedrich, Turbulent supersonic channel flow, J. Turbul. 2 (2001).

[19] Y. Morinishi, S. Tamano, K. Nakabayashi, Direct numerical simulation of compressible turbulent channel flow between adiabatic and isothermal walls, J. Fluid Mech. 502 (2004) 273–308.

[20] S. Tamano, Y. Morinishi, Effect of different thermal wall boundary conditions on compressible turbulent channel flow at M= 1.5, J. Fluid Mech. 548 (2006) 361–373.

[21] Y. Morinishi, S. Tamano, K. Nakabayashi, A DNS algorithm using B-spline collocation method for compressible turbulent channel flow, Comput. Fluids 32 (2003) 751–776.

[22] H. Foysi, S. Sarkar, R. Friedrich, Compressibility effects and turbulence scalings in supersonic channel flow, J. Fluid Mech. 509 (2004) 207–216.

[23] C. Brun, M. Boiarciuc, M. Haberkorn, P. Comte, Large eddy simulation of compressible channel flow, Theor. Comp. Fluid Dyn. 22 (2008) 189–212.

[24] L. Wei, A. Pollard, Interactions among pressure, density, vorticity and their gradients in compressible turbulent channel flows, J. Fluid Mech. 673 (2011) 1–18.

[25] L. Wei, A. Pollard, Direct numerical simulation of compressible turbulent channel flows using the discontinuous Galerkin method, Comput. Fluids 47 (2011) 85–100.

[26] E. van Driest, The problem of aerodynamic heating, Aeronaut. Engng Rev. 15 (1956) 26–41.

[27] A. Walz, Compressible turbulent boundary layers with heat transfer and pressure gradient in flow direction, J. Res. Natl. Bur. Stand. 63 (1959).

[28] L. Duan, I. Beekman, M. Martin, Direct numerical simulation of hypersonic turbulent boundary layers. Part 2. Effect of wall temperature, J. Fluid Mech. 655 (2010) 419–445.

[29] L. Duan, I. Beekman, M. Martin, Direct numerical simulation of hypersonic turbulent boundary layers. Part 3. Effect of Mach number, J. Fluid Mech. 672 (2011) 245–267.

[30] L. Duan, M. Martin, Direct numerical simulation of hypersonic turbulent boundary layers. Part 4. Effect of high enthalpy, J. Fluid Mech. 684 (2011) 25–59.

[31] E. Spina, A. Smits, S. Robinson, The physics of supersonic turbulent boundary layers, Annu. Rev. Fluid Mech. 26 (1994) 287–319.

[32] A. Demetriades, W. Martindale, Experimental determination of one-dimensional spectra in high-speed boundary layers, Phys. Fluids 26 (1983) 397–403.

[33] A. Smits, E. Spina, A. Alving, R. Smith, E. Fernando, J. Donovan, A comparison of the turbulence structure of subsonic and supersonic boundary layers, Phys. Fluids A 1 (1989) 1865–1875.

[34] B. Ganapathisubramani, N. Clemens, D. Dolling, Large-scale motions in a supersonic turbulent boundary layer, J. Fluid Mech. 556 (2006) 271–282.

[35] S. Pirozzoli, Generalized conservative approximations of split convective derivative operators, J. Comput. Phys. 229 (2010) 7180–7190.

[36] M. Bernardini, S. Pirozzoli, M. Quadrio, M. Orlandi, Turbulent channel flow simulations in convecting reference frames, J. Comput. Phys. 232 (2013) 1–6.

[37] L. Howarth, Concerning the effect of compressibility on laminar boundary layers and their separation, Proc. Roy. Soc. (London) A 194 (1948) 16–42.

[38] P. Huang, G. Coleman, van Driest transformation and compressible wall-bounded flows, AIAA J. 32 (1994) 2110–2113.

[39] H. Fernholz, P. Finley, A critical commentary on mean flow data for two-dimensional compressible turbulent boundary layers, AGARDograph 253, 1980.

[40] S. Pirozzoli, Revisiting the mixing-length hypothesis in the outer part of turbulent wall layers: mean flow and wall friction, J. Fluid Mech. 745 (2014) 378–397.

[41] R. Baidya, J. Philip, N. Hutchins, J. Monty, I. Marusic, Measurements of streamwise and spanwise fluctuating velocity components in a high Reynolds number turbulent boundary layer, Measurements 3 (2012) 7.

[42] E. van Driest, The turbulent boundary layer with variable Prandtl number, No. Amer. Avia., Inc. AL-1914, 1954.

[43] S. Pirozzoli, F. Grasso, T. Gatski, Direct numerical simulation and analysis of a spatially evolving supersonic turbulent boundary layer at M= 2.25, Phys. Fluids 16 (2004) 530–545.

[44] A. Townsend, The Structure of Turbulent Shear Flow. 2nd edn, Cambridge University Press., 1976.

[45] A. Perry, I. Marusic, A wall-wake model for the turbulence structure of boundary layers. Part 1. Extension of the attached eddy hypothesis, J. Fluid Mech. 298 (1995) 361.

[46] Y. Mizuno, J. Jiménez, Mean velocity and length-scales in the overlap region of wall-bounded turbulent flows, Phys. Fluids 23 (2011).

[47] S. Pirozzoli, On the size of the energy-containing eddies in the outer turbulent wall layer, J. Fluid Mech. 702 (2012) 521–532.

[48] N. Hutchins, I. Marusic, Evidence of very long meandering features in the logarithmic region of turbulent boundary layers, J. Fluid Mech. 579 (2007) 1–28.